To link to this article : DOI:10.1002/aic.14353
http://dx.doi.org/10.1002/aic.14353

Wicking and Evaporation of Liquids in Porous Wicks: A Simple Analytical Approach to Optimization of Wick Design

Saman Beyhaghi
Laboratory for Flow and Transport Studies in Porous Media, Dept. of Mechanical Engineering, University of Wisconsin-Milwaukee, Milwaukee, WI 53211

Sandrine Geoffroy
Université de Toulouse; UPS, INSA; LMDC (Laboratoire Matériaux et Durabilité des Constructions); 135, avenue de Rangueil; F-31077 Toulouse Cedex 04, France

Marc Prat
Université de Toulouse, INPT, UPS, IMFT, Avenue Camille Soula 31400, Toulouse, France, and CNRS, IMFT 31400, Toulouse, France

Krishna M. Pillai
Laboratory for Flow and Transport Studies in Porous Media, Dept. of Mechanical Engineering, University of Wisconsin-Milwaukee, Milwaukee, WI 53211

Wicking and evaporation of volatile liquids in porous, cylindrical wicks is investigated where the goal is to model, using simple analytical expressions, the effects of variation in geometrical parameters of a wick, such as porosity, height and bead-size, on the wicking and evaporation processes, and find optimum design conditions. An analytical sharp-front flow model involving the single-phase Darcy's law is combined with analytical expressions for the capillary suction pressure and wick permeability to yield a novel analytical approach for optimizing wick parameters. First, the optimum bead-radius and porosity maximizing the wicking flow-rate are estimated. Later, after combining the wicking model with evaporation from the wick-top, the allowable ranges of bead-radius, height and porosity for ensuring full saturation of the wick are calculated. The analytical results are demonstrated using some highly volatile alkanes in a polycarbonate sintered wick.

Keywords: wick design, porous media, wicking, imbibition, evaporation, Darcy's law, bead radius, porosity, optimization, sintered wick

Introduction

Wicking is the spontaneous transport of a liquid through a porous medium as a result of capillary suction taking place at liquid-gas interfaces at the surface or within the porous medium. Wick action is present in many engineering applications, such as heat pipes and capillary pumped loops,[1,2] propellant management devices (PMD) used in spacecraft tanks,[3] as well as in other systems made of porous sheets.[4] This is also an important phenomenon in relation with salt weathering issues in building physics, e.g., Puyate and Lawrence.[5] In almost all these examples, wicking takes place in conjunction with evaporation at the liquid-gas menisci present in the system.

Several wick-based systems are designed by consumer products companies to disperse vapors of volatile perfume or insect-repellent liquids in a room. These systems, which motivate this study, also work due to the combined action of wicking and evaporation. As sketched in Figure 1a, the wick top in such a system is usually exposed to the air so that the volatile liquid can slowly diffuse from the liquid-air interface present on top of the wick into the room air. Note that the top surface of the wick could be in level with, higher than, or lower than the surrounding casing. The evaporation phenomenon is generally improved by using local heaters placed around the wick top region so as to increase the saturation vapor pressure.

As the other systems mentioned previously, this type of system poses interesting engineering and scientific questions. In particular, we are interested in the questions concerning the design and optimization of the system. Questions such as the range of parameters allowing the system to operate with a fully liquid-saturated wick, or the parameters maximizing the wick action, are of interest in many systems. In this article, those questions are addressed for the particular system sketched in Figure 1a. It should be clear, however, that many of the results obtained in the course of the study of this particular type of systems are of broader interest.

The wicks used in consumer products applications for discharging perfume or other volatile compounds in the air are generally made by sintering. Sintering is a common industrial process for making porous wicks. For example, wicks

Correspondence concerning this article should be addressed to K. M. Pillai at Krishna@uwm.edu.

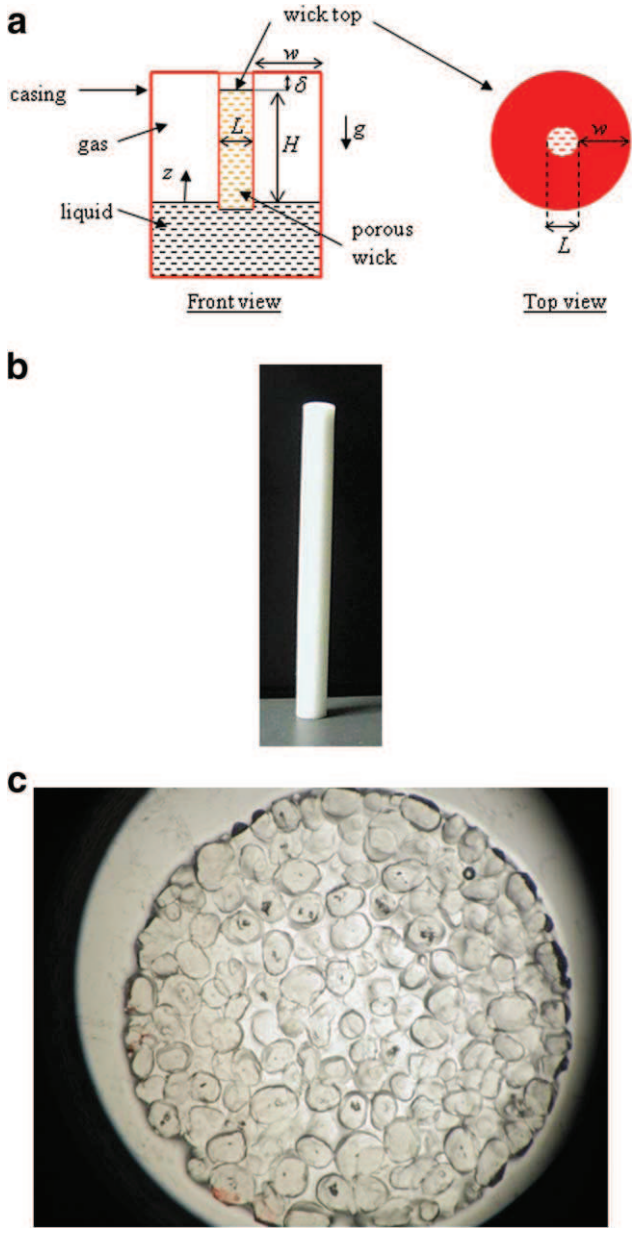

Figure 1. (a) Schematic of the system studied (without heater, with a negligible casing width *w*, and with $\delta = 0$ in most cases), (b) a typical porous wick of cylindrical shape, and (c) microstructure of a wick made from sintered polymer beads.

[Color figure can be viewed in the online issue, which is available at wileyonlinelibrary.com.]

sintered out of beads of copper or other metals are employed in heat pipes that are used for temperature-control applications.[6,7] For our system, the wick is generally obtained by sintering beads made of polymers such as polyethylene or polypropylene. This type of wick has been studied theoretically and experimentally in previous efforts. Masoodi et al.[8] developed a new model for wicking in such polymer wicks based on the single-phase Darcy's law after employing a suction pressure at the moving liquid interface. Beyhaghi et al.[9] studied the mass transport and evaporation of nondilute multicomponent liquid mixtures in the same wick. A polymer sintered wick typical of the systems considered in this article is shown in Figure 1b. The height of such a wick is typically less than 10 cm and the wick diameter is typically on the order of 5 mm. The internal microstructure of such wicks is shown in Figure 1c.

The article is organized as follows. Additional details on the problem are given after this section. The maximum wicking flow rate is investigated next. Then, wicking with evaporation at the wick top is studied in the following section. The wicking flow rate will be obtained using the Darcy's law which models single-phase flows in porous media. Using the expressions for suction pressure and permeability, the liquid flow-rate can be expressed in terms of the porosity and bead radius. The role of these two parameters in maximizing the flow rate is studied next. The optimal values for porosity and the bead size will then be obtained after balancing the wicking rate with the evaporation rate.

Problem Description

As sketched in Figure 1, the system under study consists of a porous wick which is supplied by a liquid reservoir from the bottom. The wick is cylindrical in shape, of dia. L and is made by sintering the micron-size polymer beads. Swelling of the polymer beads is neglected in the short time-frame of the wicking process, and therefore the wick can be regarded as a rigid nondeforming porous medium with a constant porosity. Furthermore, the wick is assumed to be isotropic because its flow properties are not expected to change with direction in such a particulate porous medium. Also, the wick is assumed to be fully saturated with the liquid.*

Working fluid in this study is a single-component volatile liquid. The liquid rises inside the wick due to the suction or capillary action. The gravity and viscous effects also exert their influence on the wicking liquid and tend to limit the height that can be reached by the liquid due to the capillary effects. Evaporation from the liquid-air interface is another phenomenon that accompanies wicking. Therefore, the flow rate and the position of liquid front will be determined by the interplay of these four phenomena.

In this study, the effect of increase in the ambient temperature on the wicking and evaporation rates is considered. The sides of the cylindrical wick are generally in contact with solid surfaces and therefore evaporation takes place only at the wick top.

Hexane and some other volatile alkanes are the typical chemicals used in air-fresheners and insect repellents, and therefore the results are predicted for these compounds. A wick made of polycarbonate with the average height of 75 mm and the bead radius of 20–200 μm is used in our studies. Properties of the working fluids (a group of alkanes) at room temperature are presented in Table1. (The ambient temperature and pressure are taken to be 300 K and 100 KPa, respectively.)

Wicking Flow Rate

Maximum wicking flow rate

Throughout this article, the wick is assumed to be fully saturated. Thus, we assume that the conditions are such that the liquid can be pumped up to the wick top due to wick action. Assuming the wick to be fully saturated behind a sharp interface and the use of the single-phase flow assumption is a powerful and effective simplification for modeling

*It is important to have fully-saturated wicks in commercial applications since the partially-saturated wicks are less efficient in dispersing volatile compounds in the air.

Table 1. Properties of the Working Fluids used in this Study

	Fluid properties at T=300 K				
Substance	Hexane, C_6H_{14}	Octane, C_8H_{18}	Decane, $C_{10}H_{22}$	Dodecane, $C_{12}H_{26}$	Hexadecane, $C_{16}H_{34}$
Molar mass Kg/Kmol	86	114	142	170	226
Density, Kg/m^3	655	703	735	753	773
Saturation vapor pressure, KPa	23	1.85	1.87E-1	1.76E-2	1.87E-4
Diffusivity in air, mm^2/s	8.2	6.34	5.81	5.29	4.62
Surface tension, mN/m	18.4	21.3	23.8	25.3	27.4
Dynamic viscosity, cp	0.297	0.51	0.92	1.43	3.34
Contact angle, Degrees	0	0	0	0	0

wicking in industrial wicks.[10] Using Darcy's law, the flow rate through the wick can be expressed as

$$Q=-A\frac{K}{\mu}\left(\frac{\partial P_\ell}{\partial z}+\rho g\right) \tag{1}$$

where A is the cross-section area of the wick, K is the porous medium permeability, μ is the dynamic viscosity of the liquid, ρ is the liquid density, P_ℓ is the pressure in the liquid, and z is the vertical coordinate as shown in Figure 1a. In the aforementioned equation, the gravitational term has the same sign as the pressure gradient, because the positive z-direction is chosen upward in Figure 1. Noting that $P_\ell \approx P_{atm}$ at $z=0$ (after assuming a hydrostatic pressure distribution in the liquid surrounding the wick bottom), where P_{atm} is the atmospheric pressure, Eq.1 can be expressed as

$$Q=-A\frac{K}{\mu}\left(\frac{P_\ell(H)-P_{atm}}{H}+\rho g\right) \tag{2}$$

Note that linear pressures drop within the wick, which is employed in the derivation of (2) from (1), is a direct consequence of the conservation of mass principle, i.e., $\frac{dQ}{dz}=0$

The menisci in the pores at the wick top-surface are curved so as to provide the capillary pumping effect. As a result, the liquid pressure at $z=H$ can be expressed using the Laplace's law as

$$P_\ell(H)\approx P_{atm}-\frac{2\gamma}{\xi} \tag{3}$$

where, for simplicity, we have assumed axisymmetrical menisci at the wick top; γ is the liquid surface-tension, and ξ is the menisci curvature radius, which is assumed to be the same for all menisci. This eventually leads to express (2) as

$$Q=A\frac{K}{\mu}\left(\frac{2\gamma}{\xi H}-\rho g\right) \tag{4}$$

The menisci radius ξ cannot be lower than a certain value, which corresponds to the invasion capillary-pressure threshold P_s. When the pressure difference between the gas and the liquid at a meniscus exceeds P_s, the meniscus recedes into the porous medium, and, therefore, ceases to be present at the porous surface. For a random packing of monodisperse beads of radius R_b, the capillary pressure threshold or maximum suction pressure can be expressed using an energy-balance model, obtained after equating the release of surface energy to viscous dissipation,[8,11] as

$$P_s=\frac{3(1-\varepsilon)\gamma\cos\theta}{\varepsilon R_b} \tag{5}$$

Here ε is the wick porosity, and θ is the contact angle for the air-liquid wick material system (θ should be regarded as the receding contact angle). Hence, the minimum menisci radius that is compatible with a fully saturated wick would be

$$\xi_{\min}=\frac{2\varepsilon R_b}{3(1-\varepsilon)\cos\theta} \tag{6}$$

which is obtained after taking $P_s=2\gamma/\xi_{\min}$. As a result, after using (6) with (4), the maximum flow rate the wick can pump is given by

$$Q_{\max}=A\frac{K}{\mu}\left(\frac{3(1-\varepsilon)\gamma\cos\theta}{\varepsilon H R_b}-\rho g\right) \tag{7}$$

There are several models reported in the literature where the permeability of a porous medium is expressed as a function of porosity.[12] The authors have chosen to use the general form of the Kozeny-Carman model[13,14] due to the inclusion of bead size as well as porosity

$$K=C\frac{\varepsilon^3 R_b^2}{(1-\varepsilon)^2} \tag{8}$$

Several different values for the coefficient C are available in the literature, e.g., MacDonald et al.[15] For the sintered wicks considered in this study, the corresponding permeabilities were measured by a falling head permeameter.[8] The value of fitting parameter C for each wick was determined after matching the measured permeability with the Kozeny-Carman formula and was found to be unique for each wick. Although the parameter C was found to be slightly lower than the classical value of 4/180,[15] it can be concluded from these experiments that the Kozeny-Carman model with the classical value $C=4/180$ predicts the wick permeability reasonably well. As shown by (8), the Kozeny-Carman permeability varies as the square of bead radius, whereas its variation with porosity (in the constant bead radius case)[†] increases slowly for porosities up to around 0.8 and then diverges as $\varepsilon \to 1$. These results will be used below to explain the behavior of the wicking flow-rate at different porosities and bead radii. Combining (7) and (8) finally yields

$$Q_{\max}=A\frac{C\varepsilon^3 R_b^2}{(1-\varepsilon)^2\mu}\left(\frac{3(1-\varepsilon)\gamma\cos\theta}{\varepsilon H R_b}-\rho g\right) \tag{9}$$

Equilibrium bead-radius (corresponding to $Q_{max}=0$ at the wick top)

We define the equilibrium bead-radius $R_{b.eq}$, to correspond to a pure hydrostatic equilibrium with the top menisci at their minimum radius of curvature. Under such a situation,

[†]The bead radius and porosities may be related in real sintered wicks, but for an ideal porous medium made of perfectly-spherical monodisperse particles, the two will be independent of each other for a given packing arrangement.

the liquid in the imbibed liquid-column is not moving and the upward pull on liquid column by the suction pressure is balanced exactly by the downward weight of the column. The net flow rate at the wick top is zero, and the equilibrium bead-radius can be obtained as

$$Q_{\max} = A\frac{C\varepsilon^3 R_{b.eq}^2}{(1-\varepsilon)^2\mu}\left(\frac{3(1-\varepsilon)\gamma\cos\theta}{\varepsilon H R_{b.eq}} - \rho g\right) = 0$$
$$\rightarrow R_{b.eq} = \frac{3(1-\varepsilon)\gamma\cos\theta}{\varepsilon H \rho g} \quad (10)$$

For a wick made of polymer beads and a group of alkanes (C_6H_{14}, C_8H_{18}, $C_{10}H_{22}$, $C_{12}H_{26}$ and $C_{16}H_{34}$) as the working fluids, the equilibrium bead radius is plotted in Figure 2a as a function of porosity. While there is an observable difference between the curves at small porosities, the differences are almost negligible for porosities greater than 0.4.

The same study has been done for a wick made of polymer beads with the porosity ε equal to 0.45, where the equilibrium bead-radius $R_{b.eq}$ is plotted as a function of wick height H in Figure 2b. For such a series of curves where the wick is supposed to work for all the liquids of interest, the lowest curve (hexane) should be considered for the determination of the equilibrium bead radius.

It is evident from (10) and Figure 2 that $R_{b.\mathrm{eq}}$ is inversely proportional to the porosity and the wick height, i.e., taller or "more porous" the wick, smaller the equilibrium bead-radius. Note that the suction pressure, as given by (5), is inversely proportional to the bead radius R_b; so as the bead size becomes smaller, the suction pressure becomes larger, and taller columns of liquid can be held up under these conditions.

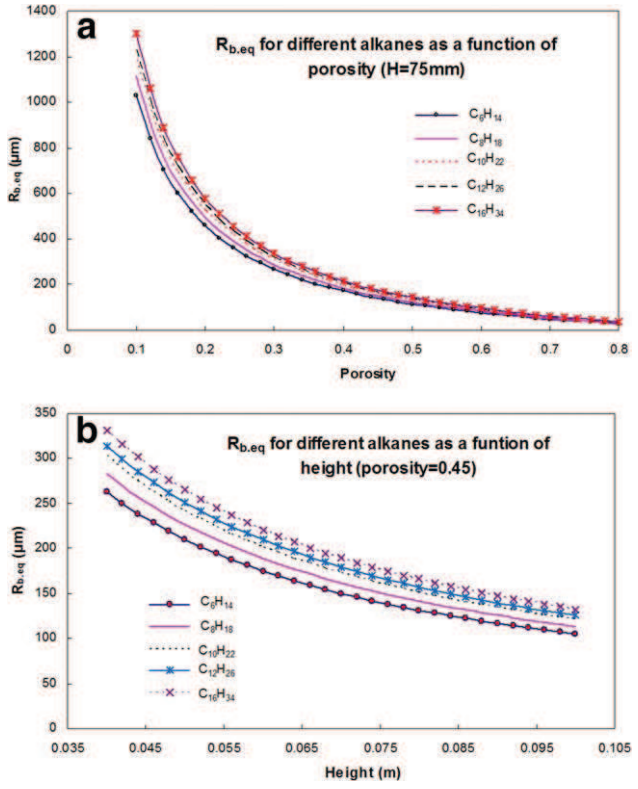

Figure 2. For a wick made of polycarbonate, and one out of a group of five alkanes as the wicking liquid, the relationship between the equilibrium bead-radius $R_{b.eq}$ and (a) the wick porosity for a wick with the height H of 75 mm, and (b) the wick height for a wick with the porosity of 0.45.

One can extrapolate the reasoning to claim that for a wick with bead radius less than $R_{b.eq}$ for a given wick height H, the wick will be able to pump the liquid with the menisci attached at the wick top, whereas this is not possible for larger bead size.[‡] So for $R_b \leq R_{b.\mathrm{eq}}$ for a given height, the wick is expected to remain fully wet although there will not be any wicking flow. The menisci at the top simply adjust their curvatures so that the capillary forces balance the gravity forces. The radius of curvature for menisci can then be estimated from (4) as

$$\xi = \frac{2\gamma}{\rho g H} \quad (11)$$

Optimal bead radius

From Eq. 9, we can see that the flow rate is a function of the bead radius in the form of a second degree polynomial. As a result, the bead size corresponding to the maximum flow rate, which the wick is capable of pumping through capillary suction to the wick top, is given by

$$\frac{dQ_{\max}}{dR_b} = 0 \rightarrow R_{b.opt} = \frac{3(1-\varepsilon)\gamma\cos\theta}{2\varepsilon H\rho g} \rightarrow R_{b.opt} = \frac{R_{b.eq}}{2} \quad (12)$$

i.e., the optimal bead-radius is half of the hydrostatic equilibrium bead-radius.

For a wick made of polycarbonate beads and with a height H, of 75 mm, the variation of the flow rate with bead radius as predicted by (9) is shown in Figure 3. In Figure 3a, the influence of porosity on flow rate of hexane is shown, whereas in Figure 3b, the porosity is set to 0.45, and the flow rate for five different alkanes is shown. It is evident that the maximum flow rate increases while the optimal bead radius decreases as the porosity increases. Figure 3b shows that with the same porosity, the wicking flow is significantly smaller for "heavier" alkanes (except for a limited bead radius range). Note that the plots are shown only for realistic values; i.e., for R_b greater than 20 μm and for positive values of $Q_{\max}$.

It is insightful to attempt some sort of nondimensionalization to present the equations in a different light. After expressing (9) for the maximum flow rate (Q_{MAX}) in terms of $R_{b.\mathrm{opt}}$, $Q_{\max}$ in (9) can be presented in terms of the dimensionless flow rate Q^*, as

$$Q^* = \frac{Q_{\max}}{Q_{MAX}} = \frac{R_b - FR_b^2}{R_{b.opt} - FR_{b.opt}^2} \quad \text{where} \quad F = \frac{\varepsilon H\rho g}{3(1-\varepsilon)\gamma\cos\theta} = \frac{1}{R_{b.eq}} \quad (13)$$

On introducing $r = R_b/R_{b.\mathrm{eq}}$ and after applying Eq.10 into Eq.13, Q^* can finally be reduced to the following elegant quadratic form

$$Q^* = \frac{Q_{\max}}{Q_{MAX}} = 4(r - r^2) \quad (14)$$

Interpretation of the two roots of Eq.14 is clear. A given flow rate $Q_{\max}$, can be obtained with two different sizes of beads. For the smaller bead size, the pressure drop due to

[‡]For $R_b > R_{b.eq.}$ the liquid front will not reach the wick top.

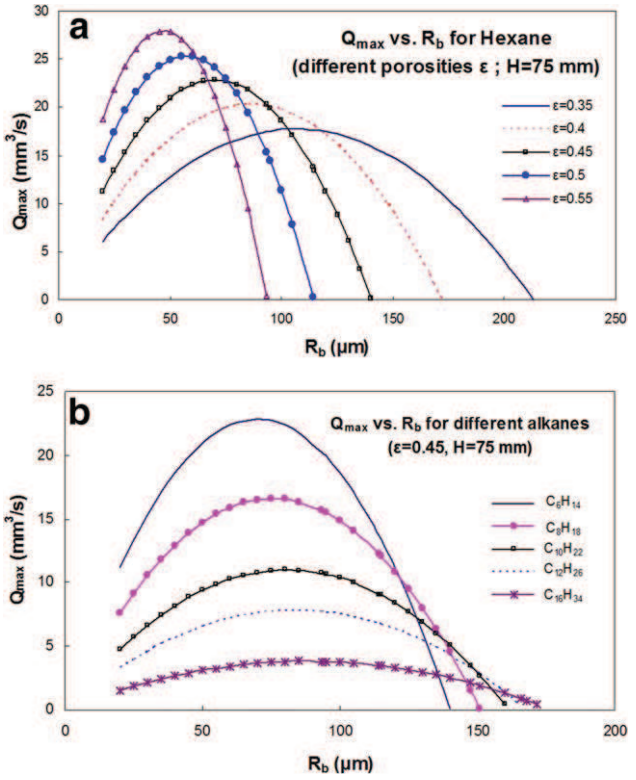

Figure 3. Variation in the volumetric wicking flow-rate Q_{max}, with the bead-radius, R_b, for a polymer wick of height $H = 75$ mm: (a) Influence of the wick porosity, and (b) influence of the working liquid properties.

Note that the bead radius corresponding to the peak of each curve is the optimal bead radius, while the point of intersection of each curve with the horizontal axis is the equilibrium bead radius for that curve. [Color figure can be viewed in the online issue, which is available at wiley onlinelibrary.com.]

viscous effects is much greater than the pressure drop due to gravity effects, and the viscous resistance is then compensated by a greater capillary suction. For the larger bead size, the viscous resistance is less but the pressure variation due to gravity effect is not negligible compared to the viscous pressure drop. The smaller viscous resistance requires, however, a smaller capillary suction compared to the solution corresponding to the smaller bead size.

Optimal porosity

Whereas random packing of monodisperse beads have porosity close to 0.45, the porosity of sintered materials can be varied over a significant range of up to 0.7 or more.[6,7] In contrast to the previous section, the bead size in the wick is kept fixed here and the effect of variation of porosity on the flow rate is studied. It is desired to obtain an optimal porosity which gives the maximum flow-rate under a constant bead-radius condition. By taking the derivative of flow rate $Q_{\max}$ at (9) with respect to the porosity, ε, while keeping other parameters such as H and R_b constant, we get

$$\frac{\partial Q_{\max}}{\partial \varepsilon} = \frac{C\varepsilon R_b}{(1-\varepsilon)^3 \mu H}\left(B\varepsilon^2 - 3B\varepsilon + 6\gamma\, Cos\theta\right) = 0 \qquad (15)$$

where B is introduced as $B = 3\gamma Cos\theta + R_b \rho g H$. The optimal porosity can then be obtained as

$$\begin{cases} \varepsilon_{opt,1} = \dfrac{3}{2} + \dfrac{\sqrt{\Delta}}{2B} \\ \varepsilon_{opt,2} = \dfrac{3}{2} - \dfrac{\sqrt{\Delta}}{2B} \end{cases} \quad \text{where} \quad \Delta = 9B^2 - 24B\gamma\, Cos\theta \qquad (16)$$

It is apparent from (16) that $\varepsilon_{\text{opt,1}}$ is greater than one, which is impossible due to the definition of the porosity. Therefore, the only possible solution for optimal porosity is

$$\varepsilon_{opt} = \frac{3}{2} - \frac{\sqrt{\Delta}}{2B} = \frac{3}{2} - \sqrt{\frac{9}{4} - \frac{6\gamma Cos\theta}{3\gamma Cos\theta + R_b \rho g H}} \qquad (17)$$

By defining a new dimensionless parameter α, the expression for optimal porosity can be simplified to

$$\varepsilon_{opt} = \frac{3}{2} - \sqrt{\frac{9}{4} - \frac{2}{1+\alpha}} \qquad (18)$$

where

$$\alpha = \frac{R_b \rho g H}{3\gamma\, Cos\theta} \qquad (19)$$

It can be easily verified that since $\alpha > 0$, the value of the optimal porosity (18) lies between zero and one. Note that the optimal porosity is determined based on the interplay of several properties incorporated in the dimensionless parameter α. Variation of the volumetric wicking flow rate with porosity is shown in Figure 4. As shown in Figure 4a (as well as indicated by Eq. 18), the optimal porosity corresponding to the maximum wicking rate decreases as the bead radius increases. In fact, the optimal porosity is quite sensitive to the bead size. Also note in Figure 4b that, under same conditions, even though the wicking rate is quite sensitive to the type of the liquid, the optimal porosity values for wicking of different alkanes of interest are only slightly different (between 0.4 and 0.46 for the group of five alkanes). Therefore, the average optimal porosity of 0.43 can be considered as a reasonable optimal porosity in this particular case. For each curve, the wicking flow rate increases with porosity until it reaches the peak, beyond which, the flow rate decreases until it reaches zero. After that, the flow rate becomes negative and hence the liquid front cannot reach the wick top.

A Limit on Wick Porosity. Using Eq. 19, the flow rate from Eq. 9 can be also expressed in terms of the porosity and α as

$$Q_{\max} = \frac{3CAR_b\gamma\, Cos\theta}{\mu H}\frac{\varepsilon^2[1-(1+\alpha)\varepsilon]}{(1-\varepsilon)^2} \qquad (20)$$

From Eq. 20, it is clear that the wick porosity has an upper limit if the wick is to remain fully wet

$$\varepsilon \le \frac{1}{1+\alpha} \qquad (21)$$

Uncertainty Analysis. In any real wick, the bead size is never a constant, but is spread over a range. Hence, we decided to study the effect of uncertainty of bead radius on the flow rate. In another study,[8] for a polycarbonate wick with the average bead radius R_b of 85.9 μm, the uncertainty in bead radius was found to be about 9.9 μm, i.e., $Rb = 85.9 \pm 9.9$ μm. This uncertainty was determined by 95% confidence level which indicates that even though the radius of the beads in a typical wick is not exactly the same

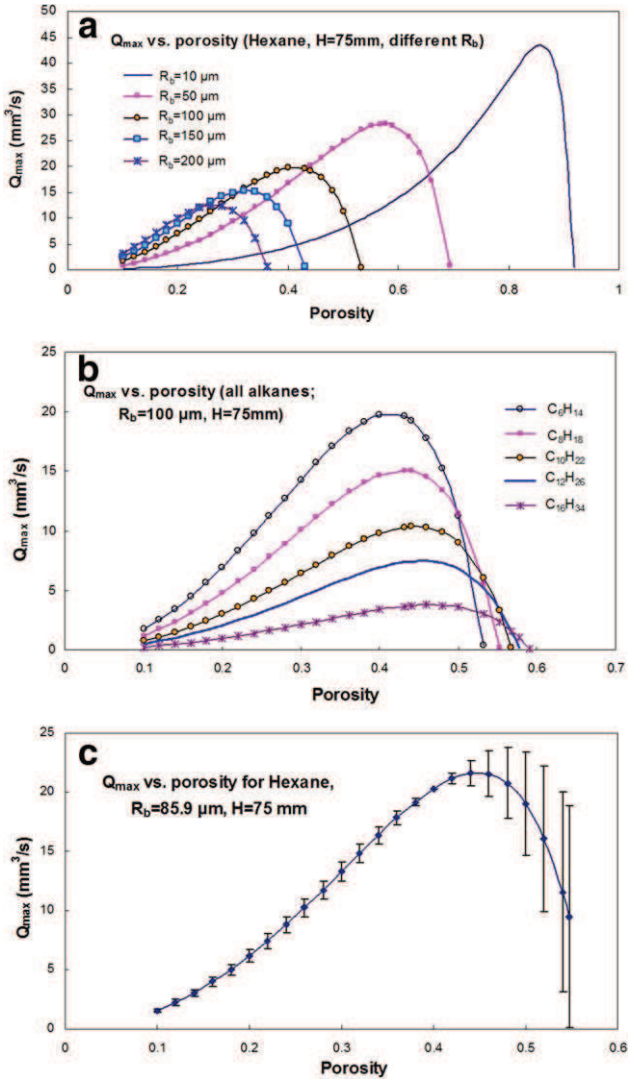

Figure 4. Variation in the wicking flow-rate Q_{max}, with the porosity for a wick made of polymer beads and having a height *H* of 75 mm: (a) Influence of bead radius on the optimal porosity, (b) influence of the liquid type on the wicking rate and optimal porosity, and (c) influence of uncertainty in bead radius on the wicking rate.

[Color figure can be viewed in the online issue, which is available at wileyonlinelibrary.com.]

everywhere and has a random distribution, we can be confident that 95% of the particles have the radius that falls in the range 85.9–9.9 $\mu m \leq R_b \leq 85.9+9.9$ μm. It should also be noted that the "95% confidence-level" corresponds to the portion of the measured beads whose radius falls within two standard deviations from the mean value of all the beads.[16]

It is expected that the uncertainty in bead radius propagates into the flow rate Q_{max}. The confidence level of the flow rate will be the same as the one for the bead radius. Neglecting the uncertainty in calculation of the other involving parameters, the uncertainty in flow rate δQ_{max} can be obtained as

$$\delta Q_{\max} = \delta R_b \frac{\partial Q_{\max}}{\partial R_b} = \delta R_b \frac{CA\varepsilon^3}{(1-\varepsilon)^2\mu}\left(\frac{3(1-\varepsilon)\gamma\cos\theta}{\varepsilon H} - 2\rho g R_b\right) \quad (22)$$

The uncertainty due to the possible random variations in bead radius is exemplified by showing the flow rate-porosity curve for flow of hexane in a 75-mm wick. The scatter bar at each porosity value is calculated from Eq. 22 and the results are shown in Figure 4c. We can be confident that the flow rate at each porosity level is somewhere along the 95% scatter bar. It is clear that at higher porosities, the scatter in the flow rate becomes larger and hence the flow rate becomes less predictable.

Flow rate as a function of porosity and bead radius

From Eq. 9, the maximum flow rate that a wick of given height H can pump is eventually given by

$$Q_{MAX} = Max(Q_{\max}) = A\frac{C\varepsilon^3 R_b^2}{(1-\varepsilon)^2\mu}\left(\frac{3(1-\varepsilon)\gamma\cos\theta}{\varepsilon H R_b} - \rho g\right) \quad (23)$$

with the bead radius and porosity to be selected as $R_b = R_{b.opt} = \frac{3(1-\varepsilon)\gamma\cos\theta}{2\varepsilon H\rho g}$ from (12), and $\varepsilon = \varepsilon_{opt} = \frac{3}{2} - \sqrt{\frac{9}{4} - \frac{2}{1+\alpha}}$ from (18), and where $\alpha = \frac{R_{b.opt}\rho g H}{3\gamma Cos\theta}$ as given in (19). The trend of curves shown in Figures 3a and 4a with variation of bead radius and porosity reveals that the maximum wicking flow rate can be achieved for extremely low-bead radii, and which leads mathematically to $\varepsilon = 1$ as the optimum porosity. Note that the use of Kozeny-Carman model for porous media with porosities close to one is not likely to be valid. Depending on the particular structure of the considered porous medium, e.g., fibrous materials or metal foams which are two examples of potentially highly porous materials, a more appropriate relationship can be selected to obtain more accurate results following the same procedure as proposed in this article In fact, the physically acceptable solution is to take the upper bound in porosity for this type of material, i.e. $\varepsilon = \varepsilon_{\max} \approx 0.7$,[7] which finally gives the optimum radius $R_b = R_{b.OPT} = \frac{3(1-\varepsilon_{\max})\gamma\cos\theta}{2\varepsilon H\rho g}$. For H of 75 mm and with Hexane as the wicking liquid, this gives $R_b = R_{b.opt} \approx 25\mu m$. However, as pointed out by the uncertainty analysis, (see Figure 4c), it is safer to select porosity slightly lower than the optimal porosity so as to limit the effect of a possible dispersion in the bead size.

Wicking with Evaporation from Wick Top

The optimal design of the wick in the absence of evaporation was investigated in the previous sections. We now wish to determine the conditions for which the liquid pumped by capillary force can balance the evaporation at the wick top. Transport mechanisms observed in this problem are (1) viscous wicking flow of the liquid due to the effect of the capillary suction, and (2) evaporation of the liquid from the wick top surface, as studied in this section. The gravity effects have also to be taken into account. A similar problem has recently been studied theoretically and experimentally in Yiotis et al.[17,18] where evaporation and capillary action were coupled. Note, however, that the main focus of this work is on the optimization of wick design using the geometrical parameters of particle size and porosity.

In the following part of the article, the conditions which lead to full saturation of the wick in the presence of evaporation from the top are investigated. Effect of three important wick parameters, i.e., bead radius, porosity, and wick height, will be studied separately, and the constraints associated

with each of them will be presented, in the subsequent subsections.

Estimate of evaporation rate E

In order to analyze the impact of evaporation on wicking, an estimate of evaporation rate is needed. From some previous efforts, it is known that a porous surface behaves as a fully wetted surface provided that the pore size d and the mean distance between pores are sufficiently small compared to the characteristic length of external mass transfer. In classical convective drying situations, this length scale is typically the mass boundary-layer thickness.[19,20] Here, the mass transfer is dominated by diffusion with possible mild free-convection effects and the relevant length scale is L, that is the size of the open side (see Eq. 24). It was recently shown that the porous surface behaves as a fully wetted surface if the pore size d is sufficiently smaller than size of the porous surface L.[21] The numerical simulation results reported therein suggest that this approximation is reasonable when the ratio L/d is greater than about 10 (assuming that the mean distance between pore is of the same order of magnitude as the mean pore size). As can be seen from Figure 1c, which shows the case of the largest beads considered in this study, this condition is satisfied for the porous wicks under consideration in this effort. Thus, the evaporation rate can be estimated as if the top surface of the wick was actually entirely covered by a thin liquid film.

The evaporation rate then depends on the condition of the surrounding air. Consider first the case where the top surface of the wick is in level with the surrounding casing ($\delta = 0$, see Figure 1a). A lower limit can be obtained by assuming an evaporation process controlled by diffusion alone[22] as

$$E = aDL\frac{M_v}{RT}P_{vs}(T) \tag{24}$$

where M_v, R, T, D and P_{vs} are the molar mass of the vapor, the gas constant, the temperature, the vapor molecular diffusion coefficient, and the saturation pressure, respectively. Note that the vapor concentration in the far field is supposed to be zero. In Eq. 24, a is a numerical factor. For a circular liquid disk of dia. L on a surface of infinite lateral extension, $a = a_\infty = 2$.[22]

However, the external mass transport given by (24) with $a \approx 2$ only represents a lower bound to the evaporation rate when the wick top is in level with the casing. As reported in Kelly-Zion et al.[23] the free-convection effects significantly increase the evaporation rate when the disk size is on the order of a few millimeters or more. According to the results reported in Kelly-Zion et al.[23] $E_{net}/E(a = 2) \approx 2$. Hence, for a disk of 5 mm dia., there is about a 100% increase in the evaporation rate (i.e., $a \sim 4$) due to the free-convection effects compared to the prediction assuming a pure diffusive transport of the vapor. Naturally, in real situations, the evaporation flux can be even greater because of the convection effects arising due to other causes (e.g., air currents, etc.). For simplicity, we assume the evaporation to be occurring in a quiescent atmosphere in this article, and, thus, use (24) to estimate the evaporation rate, but with $a \approx 4$, so as to take into account the free-convection effect.

Range of bead-radius that ensures full wick saturation

In order for the liquid to stay at the wick top, the maximum wicking mass flow rate that the wick is potentially able to pump should be equal to or greater than the evaporation rate. This constraint can be expressed as $\rho Q_{\max} \geq E$. The evaporative operating limit of the wick corresponds to the extreme case of the evaporation rate as large as the maximum wicking flow rate. The evaporation limit, thus, corresponds to $\rho Q_{\max} = E$ which by using (9) can be expressed as

$$A\frac{C\rho\varepsilon^3 R_b^2}{(1-\varepsilon)^2\mu}\left(\frac{3(1-\varepsilon)\gamma\cos\theta}{\varepsilon H R_b} - \rho g\right) = E \tag{25}$$

Rearranging and nondimensionalization of (25) leads to

$$r - r^2 = CaBo\left(\frac{H}{L}\right)^2 \tag{26}$$

where the dimensionless bead radius r, is defined as $r = R_b/R_{b.eq}$. The capillary number Ca, characterizing the competition between the capillary and viscous forces is given by $Ca = \mu E/9AC\varepsilon\rho\gamma\cos\theta$, while the bond number characterizing the competition between the capillary and gravity forces is expressed as $Bo = \rho g L^2/\gamma\cos\theta$. Two possible solutions of Eq. 26 are

$$r_1 = \frac{1}{2} - \frac{\sqrt{1 - 4CaBo(H/L)^2}}{2} \quad \text{and} \quad r_2 = \frac{1}{2} + \frac{\sqrt{1 - 4CaBo(H/L)^2}}{2} \tag{27}$$

For the maximum wicking rate to be greater than the evaporation rate, Eq. 27 changes to an inequality of the form

$$r - r^2 \geq CaBo\left(\frac{H}{L}\right)^2 \tag{28}$$

where r_1 and r_2 represent the limiting points where the maximum mass flow rate due to wicking becomes exactly equal to the evaporation rate. The points r_1 and r_2 correspond to the points of intersection of a horizontal line, representing the evaporation rate from wick top, with the "hump" of the wicking flow-rate curves. (Figures 3 and 4 show the typical "humps.") For all the bead radii between r_1 and r_2, we expect the evaporation front to stay on the wick top because the maximum wicking flow is greater than the evaporation rate. For this range of bead size, the wick is, therefore, fully saturated but with the curvature radius of the menisci at the wick top greater than the minimum value corresponding to $Q_{\max}$. Note that the menisci at the wick top adjust their curvature so that the wicking mass flow rate is equal to the evaporation rate.

Physically, the $r_2 \longrightarrow 1$ solution corresponds to R_b being sufficiently close to $R_{b.eq}$, the bead radius that ensures just enough suction pressure to keep the liquid column just touching the wick top in the absence of evaporation. For bead sizes equal to or larger than r_2, the suction pressure is not enough to pull the liquid front to the wick top and maintain it there; as a result, the final front is established somewhere below the wick top. The other solution corresponds to the viscous working limit and is obtained for sufficiently small beads. For the case $r < r_1$, the viscous drag forces are too large (due to too low of a permeability in the wick) to let the liquid move up to the wick top at a rate equal to the evaporation rate for a given suction pressure.

Influence of Temperature. The temperature can be expected to vary typically at most in the range (20–65°C) in the applications motivating this study. The saturation vapor pressure shows the most significant change with temperature

among all of the liquid properties, therefore such variation should be taken into account in calculation of the evaporation rate and consequently, the allowable bead radius range (r_1–r_2). Variation of other properties, i.e., viscosity, diffusivity in air, and surface tension with temperature is also considered using the available correlations in the literature.[24,25] The admissible dimensionless bead radius for combined wicking and evaporation of hexane from a 75-mm long wick is plotted in Figure 5a in different temperatures, ranging from 17 to 67°C (i.e., 290 to 340 K). Note that for $T = 290$ K, the product $CaBo(H/L)^2 \ll 1$. As a result $r_1 \approx CaBo\,(H/L)^2 \to 0$ and $r_2 \approx 1$. This means that the entire suitable range of wicking applies for evaporation as well. However, by increasing the temperature, this range narrows down. Therefore, for making wicks, the maximum operating temperature needs to be considered for the estimation of proper allowable bead size. In other words, the higher the operating temperature, the more restrictive is the bead-size range.

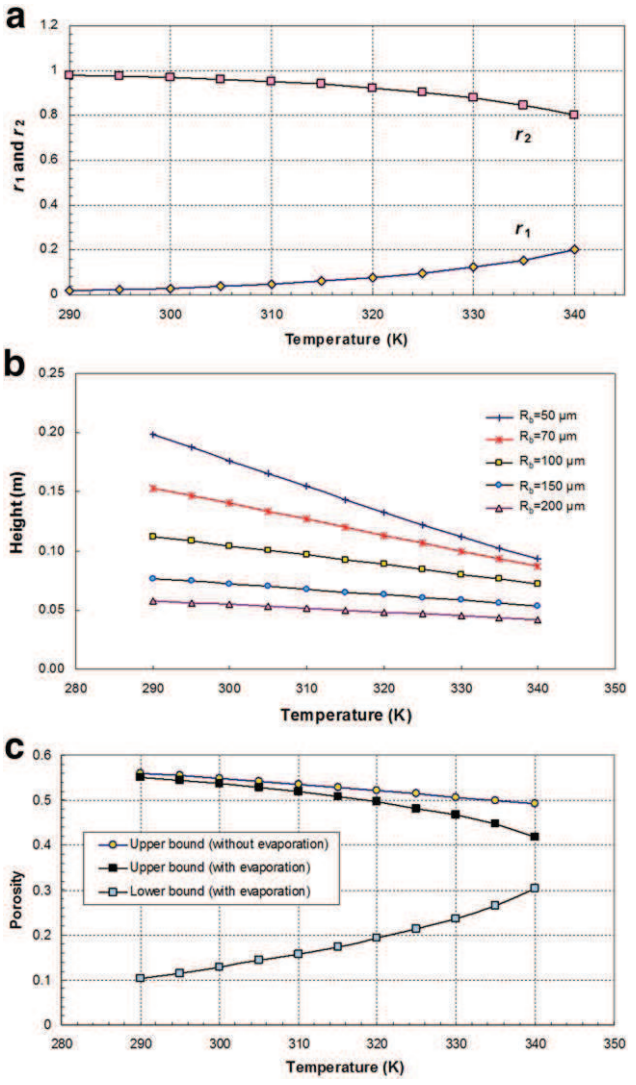

Figure 5. The influence of the ambient temperature on the allowable range of wick parameters for achieving full saturation while working with hexane: (a) dimensionless bead radius when H = 75 mm and $\varepsilon = 0.45$, (b) wick height for wicks with different bead radii and $\varepsilon = 0.45$, and (c) porosity in the absence and presence of evaporation with $H = 75$ mm and $Rb = 100$ μm.

[Color figure can be viewed in the online issue, which is available at wileyonlinelibrary.com.]

Range of wick height that ensures full saturation

In this section, we keep the bead radius and porosity constant, while estimating the maximum possible height for the wick that allows full saturation. For taller wicks, the wicking front cannot reach the top and the corresponding limiting condition would be

$$r - r^2 \geq CaBo\left(\frac{H}{L}\right)^2 \tag{29}$$

It is now important to switch from the nondimensional bead radius to the dimensional one so as to unearth the dependence of r on height H. Hence r can be rewritten as

$$r = \frac{R_b}{R_{b.eq}} = \frac{H}{H_{MAX}} \quad \text{where} \quad H_{MAX} = \frac{3(1-\varepsilon)\gamma Cos\theta}{R_b \varepsilon \rho g} \tag{30}$$

Applying (30) into (29) and solving the inequality for H leads to a range of acceptable wick heights for full wick saturation as

$$0 \leq \frac{H}{L} \leq \frac{L/H_{MAX}}{\left(CaBo + (L/H_{MAX})^2\right)} \tag{31}$$

For a commercial polymer wick with its bead radii ranging from 50 μm to 200 μm and the porosity $\varepsilon = 0.45$ while working with hexane, the allowable wick height for full saturation is shown in Figure 5b for different temperatures. While this limit is quite sensitive to temperature for small bead-radii, its variation with temperature can be neglected for the wicks with bead size greater than 200 μm. As a general trend, the admissible wick height in the presence of evaporation decreases with temperature, which is due to the increase of evaporation rate at higher temperatures.

Porosity range that ensures full wick saturation

In this part, the wick height and bead radius are considered constant, while it is desired to find the porosity range for which the wicking flow rate exceeds the evaporation rate, and therefore the liquid front stays at the wick top. By expressing the volumetric wicking flow rate at the wick top in term of the porosity ε and α—as defined in (20)—and forming the inequality $\rho Q_{\max} \geq E$, one gets

$$\rho Q \geq E \to C' \frac{\varepsilon^2[1-(1+\alpha)\varepsilon]}{(1-\varepsilon)^2} \geq E \tag{32}$$

where E has been obtained from (24) with $a = 1$, while C' is defined as

$$C' = \frac{3C\rho A R_b \gamma\, Cos\theta}{\mu H} \tag{33}$$

As a result, (32) can be rearranged as

$$(1+\alpha)\varepsilon^3 + \left(\frac{E}{C'} - 1\right)\varepsilon^2 - \frac{2E}{C'}\varepsilon + \frac{E}{C'} \leq 0 \tag{34}$$

which yields the allowable range of porosity for full wick-saturation. For the flow of Hexane in a polycarbonate wick, the range of porosity that ensures complete wick saturation is shown in Figure 5c and is compared with the porosity

limit in the absence of evaporation. While the evaporation-free problem provides only an upper limit for the admissible porosity for full wick saturation, the third-degree polynomial nature of (34) results in an upper and a lower limit for porosity. For the ambient temperature less than 300 K, the difference between the predicted upper bound of both models is negligible, whereas for higher temperatures, the porosity range for the evaporation case becomes narrower which can be again attributed to the high-evaporation rate in high-ambient temperatures. Therefore, it is advisable to choose the wick porosity in such a way that the full-saturation condition can be achieved at higher temperatures for every working liquid of interest.

Discussion

In this section, we briefly discuss the influence of several effects or parameters on the evaporation rate. The discussion is mainly based on the result of numerical computations of the evaporation rate in the diffusive limit. Some information on the numerical method of solution is given in the Appendix.

First, we explore the influence of geometrical parameters w and δ (see Figure 1a) on the evaporation rate. It is interesting to realize that these parameters do have an influence on the evaporation rate. Hence, the coefficient a in Eq. 24 depends in our case on the lateral extent of the casing, w, and the position of the wick top, δ, i.e. $a = a\ (w, \delta)$. This is illustrated in Figures 6 and 7; as can be seen, the most sensitive parameter is δ. When the wick-top surface is below the level of casing surface, i.e., when $\delta > 0$, the evaporation rate is less because of the additional mass-transfer resistance corresponding to the transport of vapor between the wick top and the entrance of the cylinder containing the wick. Although the computations were made in the diffusive limit, a quite similar effect of δ is expected when the free-convection effects are nonnegligible.

As shown in Figure 7, the effect is significant and provides a nice way of controlling the evaporation rate from the wick. For example, a "lipstick" like wick will allow controlling the evaporation rate by varying the position of the wick top in the casing.

Throughout the previous section and in the beginning of this section, we have only considered the average evaporation flux E/A. However, as shown in the appendix (see Figure A1), the evaporation flux from the wick top is not uniform when δ is sufficiently small. In this case, it is likely that the menisci begin to recede first at the periphery of the wick-top surface since this is where the evaporation flux is the greatest. A more detailed analysis is clearly needed in this case to evaluate more accurately the working limits of a fully saturated wick.

Using a wick of square (or polygonal) cross section in a casing tube also of square (or polygonal) cross section instead of round cross section could be interesting for some applications. The corners in this type of geometry favor the development of capillary liquid films that can greatly affect the evaporation rate (when $\delta > 0$), i.e., Chauvet et al.[26] Depending on the application, one may be willing to avoid this film effect so as to control the evaporation rate when playing with δ, or, on the contrary, to favor the development of capillary liquid-films as an additional parameter for obtaining desired evaporation rates.

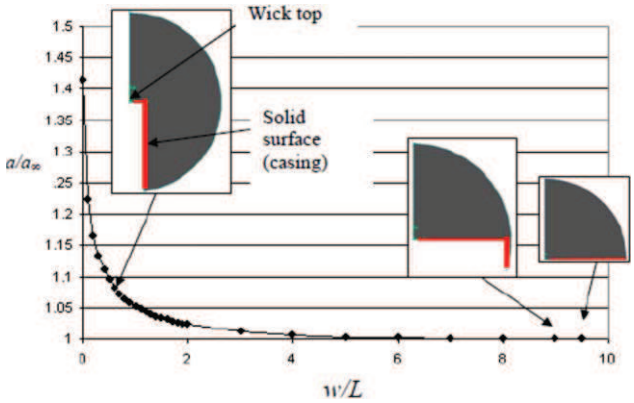

Figure 6. Variation in the evaporation-rate prefactor, *a*, as a function of the casing thickness, *w*; a_∞ is the value of the prefactor for an unbounded solid surface ($a_\infty = 2$).

The insets show a sketch of the computational domains (in gray). As can be seen, the evaporation rate is very close to the one for an infinite lateral surface ($w \to \infty$) when w/L is greater than about 4. These results are obtained assuming a purely diffusive vapor-transport. [Color figure can be viewed in the online issue, which is available at wileyonlinelibrary.com.]

Summary and Conclusion

The phenomenon of wicking and evaporation in a cylindrical porous wick made of sintered polymer beads was studied in this article. Darcy's law for liquid flow behind a clearly defined liquid front was employed, along with the Kozeny-Carman model for permeability and the energy

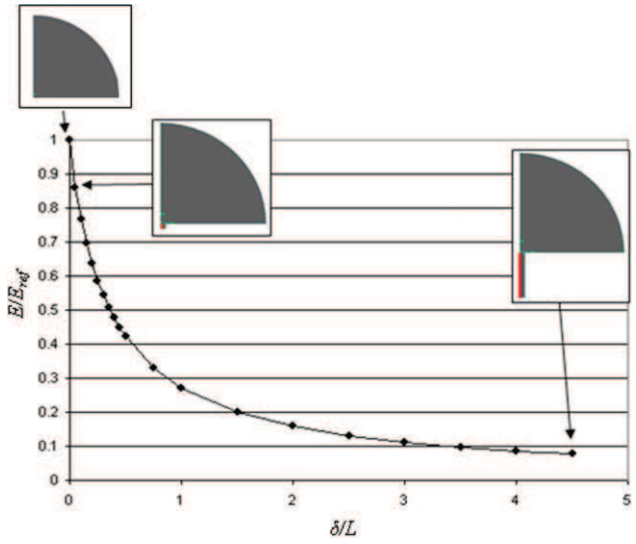

Figure 7. Influence of the wick-top position, δ, from the casing top surface on the evaporation rate from the wick top.

E_{ref} is the evaporation rate for $\delta = 0$ (the wick-top surface in level with the casing top surface). Note that $w = 0$ in this example. Similar results are obtained when $w > 0$. As seen earlier, the evaporation rate decreases nicely with the position of the wick top in the casing, which provides a way of controlling the evaporation rate. The sensitivity to the position is particularly marked for δ in the range (0, L). These results are obtained assuming a purely diffusive vapor-transport. [Color figure can be viewed in the online issue, which is available at wileyonlinelibrary.com.]

balance model for suction pressure at the liquid front. The primary goal of this work was to study the effects of variations in porosity and mean bead-radius of the wick on the wicking flow rate and to determine the optimal values corresponding to the maximum wicking flow rate inside the wick. The optimal bead-radius was found to be half of the equilibrium bead-radius which is the maximum radius that lets the liquid front reach the wick top. The optimal porosity (for maximizing the wicking flow rate) was also found for different working liquids and for the wicks with different bead radii.

The fully saturated wick undergoing evaporation from the top was considered next and a practical range of bead radius needed to keep the wick completely wet was found. This bead-radius range was needed for the wick to generate enough suction pressure to pump the liquid to the top of the wick and maintain the liquid front there. For the flow of the liquids as volatile as Hexane in a Polycarbonate porous wick with 75 mm height, the range of bead radii is observed to be almost the entire wicking-allowable range in the ambient temperature of 300 K, but it narrows down due to the rapid increase of evaporation as the ambient temperature is raised to near boiling temperature (340 K). It was also seen that the maximum height of the wick that allows full saturation in the presence of evaporation decreases almost linearly with temperature, while the slope of the line depends on bead radius. Finally, the variation in the porosity range for ensuring full wick saturation (for constant wick height and bead size) was studied both in the absence and the presence of evaporation.

The results of this study will help the industrial users of commercial wicks to consider the effects of the liquid type, operating temperature, and geometrical parameters of the wick, such as porosity, bead size and height, on the rate of liquid flow inside the wick as well as on the rate of liquid evaporation and the conditions for keeping the wick fully-saturated.

Notation

A = cross-sectional area of the wick, m^2
a = dimensionless prefactor for evaporation rate, as used in Eq. 24
B = intermediate parameter defined as $B=3\gamma Cos\theta+R_b\rho gH$, N/m
Bo = bond number defined as $Bo=\rho gL^2/\gamma\cos\theta$
Ca = capillary number defined as $Ca=\mu E/9AC\varepsilon\rho\gamma\cos\theta$
C = the permeability constant for the Kozeny-Carman model, Eq. 8
C' = an intermediate parameter defined in Eq. 33, kg/s
D = diffusion coefficient of vapor in air, m^2/s
d = pore diameter in the model porous surface, m
E = evaporation rate, kg/s
F = intermediate parameter defined in Eq. 13, m^{-1}
g = gravitational acceleration, m/s^2
H = wick height, m
j = evaporation flux as defined in the Appendix, Figure A1 caption, kg/s-m^2
j_0 = evaporation flux at the center of wick top, kg/s-m^2
K = permeability of the wick, m^2
L = wick diameter, m
M_v = molar mass of vapor, kg/Kmol
P_ℓ = pore-averaged liquid pressure, Kpa
P_{atm} = atmospheric pressure, Kpa
P_s = suction pressure, Kpa
P_{vs} = saturation vapor pressure, Kpa
Q = volumetric wicking flow rate, m^3/s
Q^* = dimensionless volumetric wicking flow rate as defined in Eq. 13
Q_{max} = maximum volumetric wicking flow-rate (corresponding to the minimum curvature radius), m^3/s
r = dimensionless bead radius defined as $R_b/R_{b.eq}$; also radial coordinate in the Appendix, Figure A1 caption, m
R = universal gas constant, kJ/Kmol-K
R_b = mean bead radius, m
T = temperature, K
w = casing width, m
z = vertical coordinate in the wetted wick, m

Greek letters

α = dimensionless parameter defined in Eq. 19
γ = liquid surface tension, N/m
Δ = intermediate parameter defined in Eq. 16, N^2/m^2
δ = wick-top position measured from the casing top, m
δQ = small variation (uncertainty) in Q
δR_b = small variation (uncertainty) in the bead radius
ε = wick porosity
ξ = curvature radius of surface menisci, m
μ = dynamic viscosity of the liquid, Pa.s
ρ = density of the liquid, kg/m^3
θ = contact angle

Subscripts

eq = equilibrium
m = meniscus
min = minimum
max = maximum
MAX = maximum of all the maxima
opt = optimum
OPT = optimum of all the optima
Ref = reference
S = solid; also: saturation
∞ = far field

Literature Cited

1. Faghri A. *Heat Pipe Science and Technology*. New York: Taylor &Francis; 1995.
2. Paterson GP. *An Introduction to Heat Pipes: Modeling, Testing, and Applications*. 1st ed. New York: Wiley Interscience; 1994.
3. Fries N, Odic K, Conrath M, Dreyer M. The effect of evaporation on the wicking of liquids into a metallic weave. *J Colloid Interface Sci*. 2008;321:118–129.
4. Lockington DA, Parlange JY, Lenkopane M. Capillary absorption in porous sheets and surfaces subject to evaporation. *Trans Porous Media*. 2007;68:29–36.
5. Puyate YT, Lawrence CJ. Steady state solutions for chloride distribution due to wick action in concrete. *Chem Eng Sci*. 2000;55:3329–3334.
6. Leong KC, Liu CY, Lu GQ. Characterization of sintered copper wicks used in heat pipes. *J Porous Mater*. 1997;4:303–308.
7. Xin GM, Cui KH, Zou Y, Cheng L. Development of sintered Ni-Cu wicks for loop heat pipes. *Sci China Ser E-Tech Sci*. 2009;52:1607–1612.
8. Masoodi R, Pillai KM, Varanasi PP. Darcy's law based models for liquid absorption in polymer wicks, *AIChE J*. 2007;53:2769–2782.
9. Beyhaghi S, Pillai KM, Qadah DT, Dietz ML. Evaporation and transport of non-dilute, multi-component liquid mixtures in porous wicks: Simulation and experimental validation. *Int J Heat Mass Transfer*. 2011;54:5216–5230.
10. Masoodi R, Pillai KM. Single-phase flow (sharp-interface) models for wicking. In: Masoodi R, Pillai KM. *Wicking in Porous Materials: Traditional and Modern Modeling Approaches*. Boca Raton, FL: Taylor & Francis Group; 2012:97–130.
11. Masoodi R, Pillai KM. A general formula for capillary suction pressure in porous media. *J Porous Media*. 2012;15:775–783.
12. Pillai KM, Hooman K. An introduction to modeling flows in porous media. In: Masoodi R, Pillai KM. *Wicking in Porous Materials: Traditional and Modern Modeling Approaches*. Boca Raton, FL: Taylor & Francis Group; 2012:55–96.
13. Kozeny J. Uber Kapillare Leitung des Wassers im Boden, Sitzungsberichte. Royal Academy of Science, Vienna, *Proc. Class I*. 1927; 136:271–306.
14. Carman, PC. Fluid flow through a granular bed. *Trans Inst Chem Eng London*. 1937;15:150–156.
15. Macdonald IF, El-Sayed MS, Mow K, Dullien FAL. Flow through porous media-the ergun equation revisited. *Ind Eng Chem Fundam*. 1979;18:199–208.

16. Wheeler AJ, Ganji AR. *Introduction to Engineering Experimentation*. Upper Saddle River, NJ: Prentice Hall; 1996.
17. Yiotis AG, Salin D, Tajer ES, Yortsos YC. Analytical solutions of drying in porous media for gravity-stabilized fronts. *Phys Rev E*. 2012;85:046308.
18. Yiotis AG, Salin D, Tajer ES, Yortsos YC. Drying in porous media with gravity-stabilized fronts: Experimental results. *Phys Rev E*. 2012;86:026310.
19. Suzuki M, Maeda S. On the mechanism of drying of granular beds. *J Chem Eng Japan*. 1968;1:26–31.
20. Yiotis AG, Tsimpanogiannis IN, Stubos AK, Yortsos YC. Coupling between external and internal mass transfer during drying of a porous medium. *Water Res Res*. 2007;43:W06403.
21. Veran-Tissoires S, Geoffroy S, Marcoux M, Prat M. Evaporation and wicking. In: Masoodi R, Pillai KM. *Wicking in Porous Materials: Traditional and Modern Modeling Approaches*. Boca Raton: Taylor & Francis Group; 2012:201–236.
22. Picknett RG, Bexon R. The evaporation of sessile or pendant drops in still air. *J Colloid Interface Sci*. 1997;61:336–350.
23. Kelly-Zion PL, Pursell CJ, Vaidya S, Batra J. Evaporation of sessile drops under combined diffusion and natural convection. *Colloids Surfaces A Physicochem Eng Aspects*. 2011;381:31–36.
24. Thermodynamics and Properties Lab. Dept. of Chemical Engineering, Korea Univerity. Korea thermophysical properties Data Bank. http://www.cheric.org/kdb/. Accessed September 1, 2012.
25. Aguila-Hernandez J, Hernandez I, Trejo A. Temperature dependence of the surface tension for binary mixtures of n-butanenitrile +n-alkanes. *Int J Thermophys*. 1995;16:45–52.
26. Chauvet F, Duru P, Geoffroy S, Prat M. Three periods of drying of a single square capillary tube. *Phys Rev Lett*. 2009;103:124502.
27. Hu H, Larson RG. Evaporation of a sessile droplet on a substrate. *J Phys Chem B*. 2002;106:1334–1344.

Appendix A: Computation of Evaporation Flux Distribution in the Diffusive Limit

The results depicted in Figures 6 and 7, and the ones presented in this appendix, are obtained by solving the Laplace equation governing the vapor concentration field in the pure diffusive limit around the system formed by the wick and the casing. The numerical simulations are performed using FLUENT, the computational fluid dynamics analysis package by ANSYS. We impose the vapor concentration corresponding to a liquid surface on the wick top, zero flux condition on solid surface, and a zero concentration in the far field. The two-dimensional (2-D) axisymmetrical computational domain corresponds to a spherical outer domain around the system. Numerical tests have shown that it is sufficient to consider a sphere with a radius = 10 L to obtain a solution independent of the sphere radius. Further numerical details will not be given here since this is not the main focus of the article. The interested reader can find further details in Veran-Tissoires et al.[21] Comments are given in the figure caption (Figure A1).

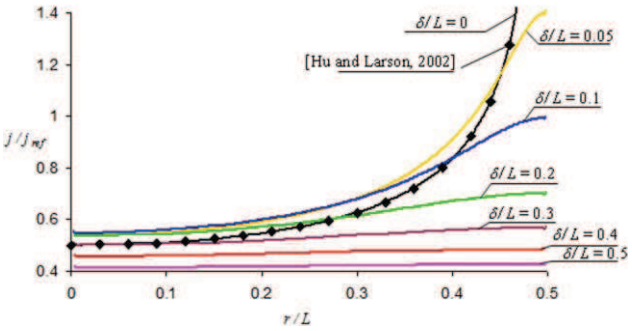

Figure A1. Influence of the wick-top position δ, from the casing-top surface on the radial distribution of evaporation flux at the porous wick-top.

Here, r is the radial position on the wick-top surface such that $r/L = 0.5$ corresponds to the wick-top surface periphery and $r/L = 0$ to the center of the wick top surface. The reference flux $j_{ref} = E/(\pi L^2/4)$ with E computed using Eq. 24 with $a = 2$ (diffusive limit). As can be seen, the evaporation flux is much greater at the periphery of the wick-top surface when δ is small. By contrast, the evaporation flux is uniform when δ is on the order of the wick radius ($\delta/L = 0.5$) or larger. The black diamond symbols in the figure (◆) represent the analytical result obtained using the expression $j(r) = j_0\left[1-(2r/L)^2\right]^{-1/2}$ where $j_0 = \frac{4DP_{vs}M_v}{\pi LRT_w}$,[27] which applies to the case $\delta = 0$. The excellent agreement between our numerical computations (black solid line) and this analytical expression confirms the quality of the numerical computations.